Mechanistic Insights into CO$_2$ Conversion to CO Using Cyanide Manganese Complexes

Mechanistic Insights into CO₂ Conversion to CO Using Cyano Manganese Complexes

Kailyn Y. Cohen, Delaan G. Nedd, Rebecca Evans, and Andrew B. Bocarsly*

Department of Chemistry, Frick Laboratory, Princeton University, Princeton, New Jersey, United States

Abstract

Without the use of a photosensitizer, [Mn(bpy)(CO)$_3$(CN)] (**MnCN**) can photochemically form [Mn(bpy)(CO)$_3$]$^-$, the active species for CO$_2$ reduction. While cases of the axial X-ligand dissociating upon irradiation of *fac*-M(N-N)(CO)$_3$X complexes (M = Mn or Re; N-N = bipyridine (bpy) ligand; X = halogen or pseudohalogen) are well documented, the axial cyanide ligand is retained when either [Mn(bpy)(CO)$_3$(CN)] or [Mn(mesbpy)(CO)$_3$(CN)], **MnCN(mesbpy)**, are irradiated anaerobically. Infrared and UV-vis spectroscopies indicate the formation of [Mn(bpy)(CO)$_2$(MeCN)(CN)] (**s-MnCN**) as the primary product during the irradiation of **MnCN**. An in-depth analysis of the photochemical mechanism for the formation of [Mn(bpy)(CO)$_3$]$^-$ from **MnCN** is presented. **MnCN(mesbpy)** is too sterically hindered to undergo the same photochemical mechanism as **MnCN**. However, **MnCN(mesbpy)** is found to be electrocatalytically active for CO$_2$ reduction to CO. Providing an interesting distinction between photochemical and electrochemical charge transfer.

Introduction

Atmospheric carbon dioxide levels continue to increase from the burning of fossil fuels, leading to global warming and climate change.[1, 2] One attractive solution is to remove CO_2 from the environment and transform it either electro- or photochemically using molecular catalysts.[3] The reduction of CO_2 is challenging both kinetically and thermodynamically, as linear CO_2 must rehybridize or "bend" when accepting an electron.[4, 5] However, several molecular electrocatalysts utilizing transition metals have been reported that can achieve CO_2 reduction.[6-12] Of interest is the transformation of CO_2 to CO, a main component in synthesis gas (CO + H_2), which can be used to obtain other fuels through Fischer-Tropsch processes.[13, 14] In particular, *fac*-[M(N-N)(CO)$_3$X] complexes (M = Mn or Re; N-N = bipyridine (bpy) ligand; X = halogen or pseudohalogen) are of interest because of their tunability and affinity for CO_2 reduction over hydrogen evolution. While much attention has been given to the Re versions of these catalysts,[15-17] Mn is a viable first row alterative of pragmatic interest because of its significantly higher natural abundance and lower electrochemical overpotentials.[18, 19]

The complex, *fac*-[Mn(bpy)(CO)$_3$Br] (**MnBr**) was first reported by Bourrez *et al.* in 2011, to be an electrocatalyst for CO_2 reduction in the presence of weak Bronsted acids.[19, 20] The initial one-electron reduction of **MnBr** places an electron in a bipyridine-based π^*-orbital, which is then thought to be thermally excited into a Mn-based σ^* manifold of orbitals.[21, 22] This leads to Br$^-$ ligand loss and formation of the metal-metal bonded dimer[Mn(bpy)(CO)$_3$]$_2$.[20, 23, 24] Subsequent reduction of this dimer has then been suggested to produce the active species for CO_2 reduction, [Mn(bpy)(CO)$_3$]$^-$.[20] Many groups, including ours, have reported alterations of the polypyridyl framework by adding substituents to the bpy backbone, adding pendant H-bond donors, or by using NHC-ligands.[10, 25-31]

Due to their apparent extreme light sensitivity, and in contrast to the noted electrochemical studies, Mn tricarbonyl complexes have been underexplored as CO_2 photoreducing agents, unless utilized in tandem with a photosensitizer to avoid the direct photochemical formation of a **MnBr** excited state.[32-35] However, we have reported that when **MnBr** is irradiated in the absence of oxygen, a Mn-Mn dimer is formed. If oxygen is present, then the complex degrades, releasing CO ligands.[36] While axial ligand substitution can alter the rate of photodegradation under room light in the presence of oxygen,[37] it cannot be completely eradicated. This finding highlights the importance of using $^{13}CO_2$ when studying this class of compounds photochemically, since free CO formed by ligand release, must be deconvoluted from CO formed by the reduction of CO_2.

Recently, we reported on the photochemical transformation of a cyanide-bridged dimer,[38] [bpy(CO)$_3$Mn(μ-CN) Mn bpy(CO)$_3$]$^+$ **Mn$_2$CN$^+$**, that was able to transform CO_2 into CO without a photosensitizer.[36, 38] These results suggested a further exploration of the effects of cyanide ligation on the photoevolution of Mn(I) tricarbonyl complexes. Herein, the mechanism for the formation of the doubly reduced catalytically active species, [Mn(bpy)(CO)$_3$]$^-$, upon irradiation of **MnCN** is presented. In contrast, it is found that its bulky counterpart, **MnCN(mesbpy)**, is not able to form the doubly reduced species photochemically, as multiple bimolecular processes are slowed by the steric hindrance of this complex. In contrast, electrochemically, **MnCN(mesbpy)** is able to produce a remarkable 1:1 ratio of ^{13}CO:^{12}CO from $^{13}CO_2$, as opposed to the typical 1:3 ratio associated with **MnCN and MnBr**.[39] Thus, the steric constraints of this complex play very different roles in its photochemical versus electrochemical reduction chemistry.

Results and Discussion

Synthesis and Characterization

The UV-vis absorption spectra for **MnBr**, **MnBr(mesbpy)**, **MnCN**, and **MnCN(mesbpy)** in acetonitrile (MeCN) are shown in **Figure 1**. **MnCN(mesbpy)** has an MLCT band centered at 380 nm ($\varepsilon = 2285$ M^{-1} cm^{-1}), which is the same value as the MLCT band for **MnCN**. Thus, the relative energies between the Mn(I) d-π orbitals and the ligand-based π^* orbitals are the same. The CN-ligated complexes both display higher energy MLCT bands than the Br-ligated complexes: MnBr has an absorption at 417 nm and **MnBr(mesbpy)** at 390 nm.
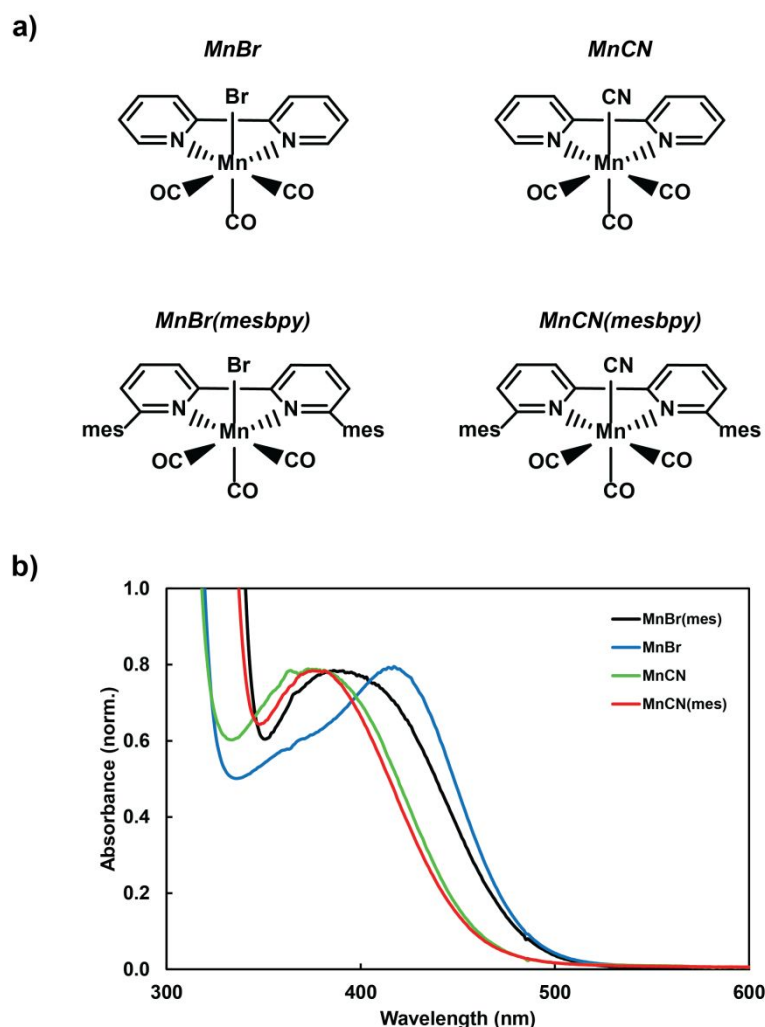
a)

b)

Figure 1. a) Representation of and b) UV-vis absorption spectra of the complexes, MnBr, MnBr(mesbpy), MnCN, and MnCN(mesbpy), at 298 K using 1 cm path length.

4

The IR absorption spectra for **MnBr**, **MnBr(mesbpy)**, **MnCN**, and **MnCN(mesbpy)** in

acetonitrile (MeCN) are shown in **Figure 2b.** The calculated spectrum in **Figure 2a** shows good

agreement with the liquid-phase IR spectrum for **MnCN(mesbpy)**. At around 1940 cm^{-1} in the

calculated spectrum, there are two non-degenerate signals that are associated with the

asymmetric (1944 cm^{-1}) and symmetric (1943 cm^{-1}) equatorial stretches. The ATR-IR spectra of

the four complexes in the solid-state are located in **Figure S1**. **MnCN** and **MnCN(mesbpy)** both

display a terminal cyanide stretch at 2115 cm^{-1}. The two stretches at lower wavenumbers

correlate to the asymmetric and symmetric stretches of the two equivalent, equatorial

carbonyls.[40] Interestingly, these two stretches for **MnBr(mesbpy)** are 25 cm^{-1} apart, located at

1909 and 1934 cm^{-1}, whereas they overlap in solution for **MnCN(mesbpy)**, located at 1930 cm^{-1}.

For the CN-ligated counterparts, the carbonyl peaks are shifted to slightly higher wavenumbers.

This is consistent with the π-accepting ability of cyanide which competes with the carbonyl

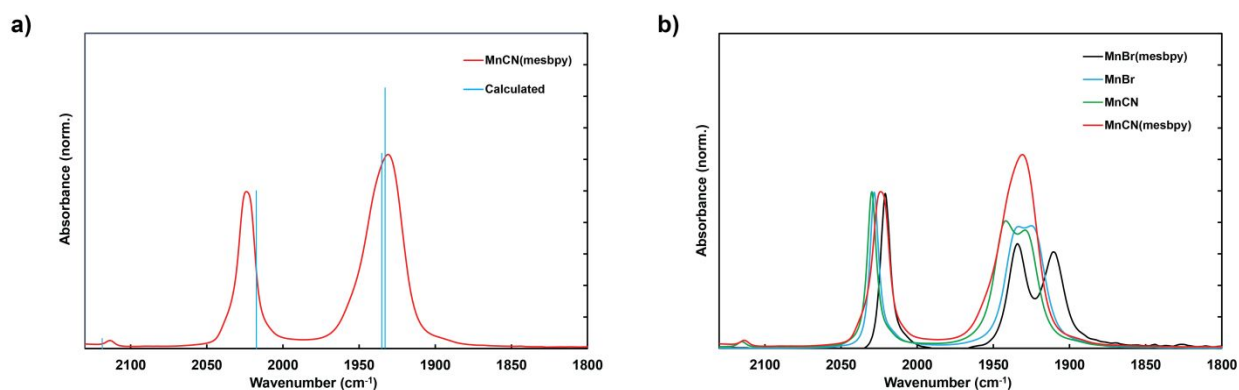ligands for back bonding electron density.

Figure 2. a) Calculated and experimental liquid-phase IR absorption spectrum for
MnCN(mesbpy) and b) IR absorption spectra for **MnBr**, **MnBr(mesbpy)**, **MnCN**, and
MnCN(mesbpy) in acetonitrile.

The ^{13}C NMR spectrum of **MnCN(mesbpy)** in DMSO-d$_6$ (**Figure S3**) resembles that of

the ^{13}C NMR assignment for **MnCN.** [41] Two equatorial carbonyl carbons are located at 215.5

ppm, one axial carbonyl carbon is at 213.4 pm, and the terminal cyanide carbon is located at

163.8 ppm.

MnCN(mesbpy) was recrystallized by layering diethyl ether over CH_2Cl_2 in the dark at

room temperature. The molecular structure of **MnCN(mesbpy)** from single crystal X-ray

diffraction is shown in **Figure 3**. Relevant bond lengths for related manganese tricarbonyl
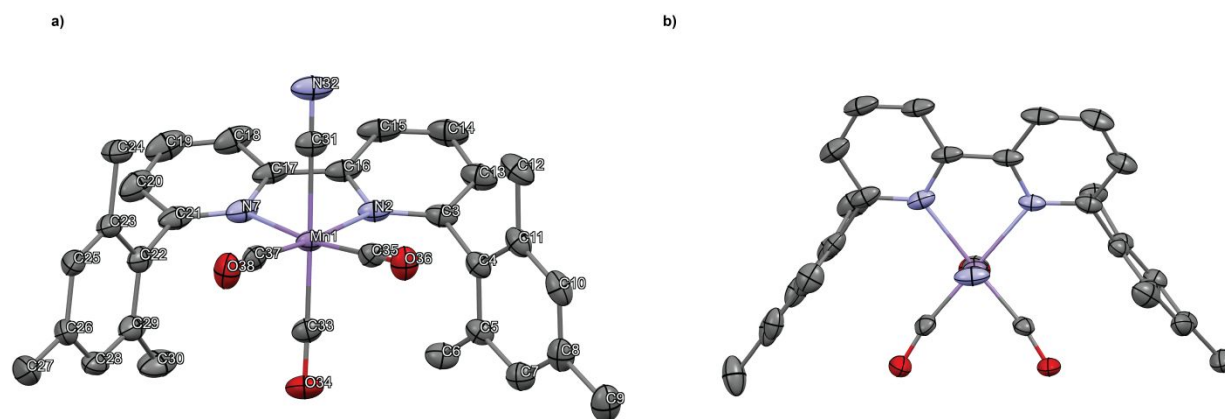
species are displayed in **Table 1**.

Figure 3. a) Molecular structure of Mn(mesbpy)(CO)₃CN with ellipsoids set at 50% probability
and b) looking down the axial bond. Hydrogen atoms and CH_2Cl_2 have been omitted for clarity.
Selected bond lengths (Å): Mn1-N2, 2.099(2); Mn1-C37, 1.804(3); Mn1-C35, 1.803(3); Mn1-
C33, 1.832(2); Mn1-C31, 2.003(2); Mn1-N7, 2.087(2).

Compared to **MnBr(mesbpy)**, **MnCN(mesbpy)** has a shorter Mn-X bond length as

expected due to Mn π-backbonding to the cyanide ligand, strengthening the Mn-CN bond, and

the larger radius of the Br compared to C. Since the axial carbonyl, *trans* to the cyanide ligand

competes for the same electron density, π-backbonding was weaker to this ligand, resulting in a

longer Mn-CO$_{axial}$ bond. The bond angle formed by C35-Mn-C37 is 81.2^0 and is in good

agreement with the bond angle obtained from the DFT calculated optimized geometry (80.5^0).

Coordinates for the crystal structure and for the DFT are located in the SI.

Table 1. Selected bond lengths of **MnCN**,[42] **MnBr(mesbpy)**,[28] and **MnCN(mesbpy)** from x-ray diffraction.

	Bond length (Å)		
	MnCN	**MnCN(mesbpy)**	**MnBr(mesbpy)**
Mn-X$_{axial}$	1.988 ± 0.004	2.003 ± 0.002	2.5298 ± 0.0006
Mn-CO$_{axial}$	1.829 ± 0.004	1.832 ± 0.002	1.795 ± 0.002

Photochemistry

MnCN was irradiated at 395 nm (2.97×10^{-9} einstein per s intensity), exciting the Mn d-π →bpy π* transition, in dry and degassed MeCN. Liquid-phase IR (**Figure 4**) confirmed the formation of [Mn(bpy)(CO)$_2$(MeCN)(CN)], abbreviated **s-MnCN**, within the first five seconds of irradiation. The small peak at 2081 cm^{-1} is a terminal cyanide stretch and the two carbonyl peaks are located at 1933 and 1858 cm^{-1}, which are more easily seen in the difference IR spectrum (**Figure S4**).
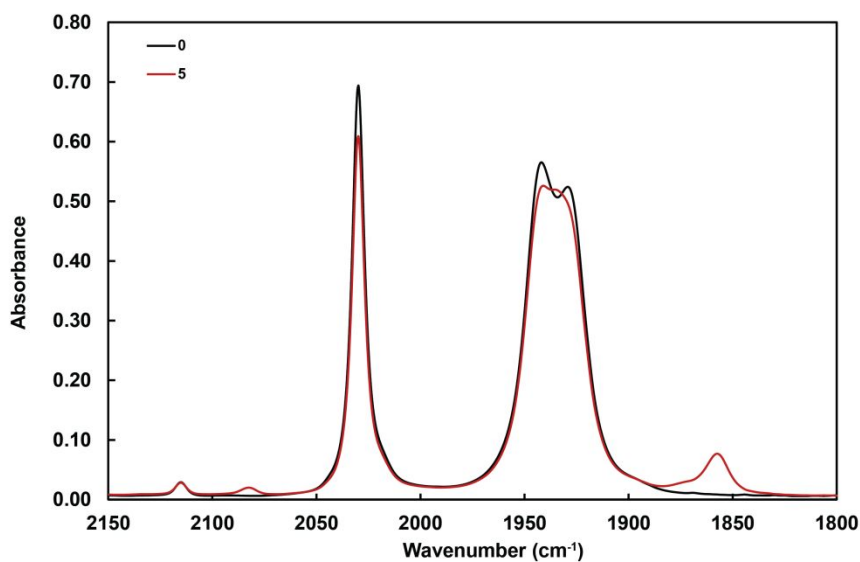

Figure 4. Liquid phase IR spectrum in degassed MeCN, before and after five seconds of irradiation with a 395 nm LED (2.97×10^{-9} einstein per s intensity), showing a shift in the terminal CN peak to 2081 cm^{-1} and a new peak at 1858 cm^{-1}.

The proposed structure of **s-MnCN** is shown in **Figure 5**, where the solvent ligand replaces an

equatorial carbonyl, and is based on similar dicarbonyl species.[43, 44] Additionally, in a separate

irradiation experiment where PPh3 is present, the phosphine ligand replaces an equatorial

carbonyl, rather than the cyanide ligand, which is consistent with the photochemical work done

by Gómez *et al.* (**Figures S6-S7**).[41] It has previously been reported that irradiating

[Mn(bpy)(CO)3Br] causes Br- loss followed by dimerization to form [Mn(bpy)(CO)3]2.[23] Thus, in

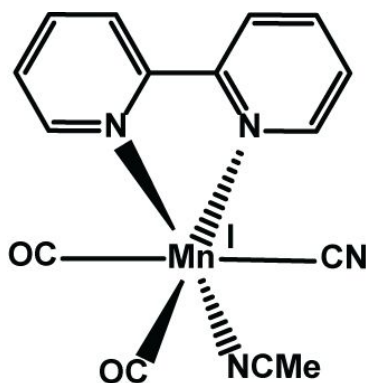contrast to [Mn(bpy)(CO)3Br], irradiation of **MnCN** displaces a CO ligand, not the X ligand.

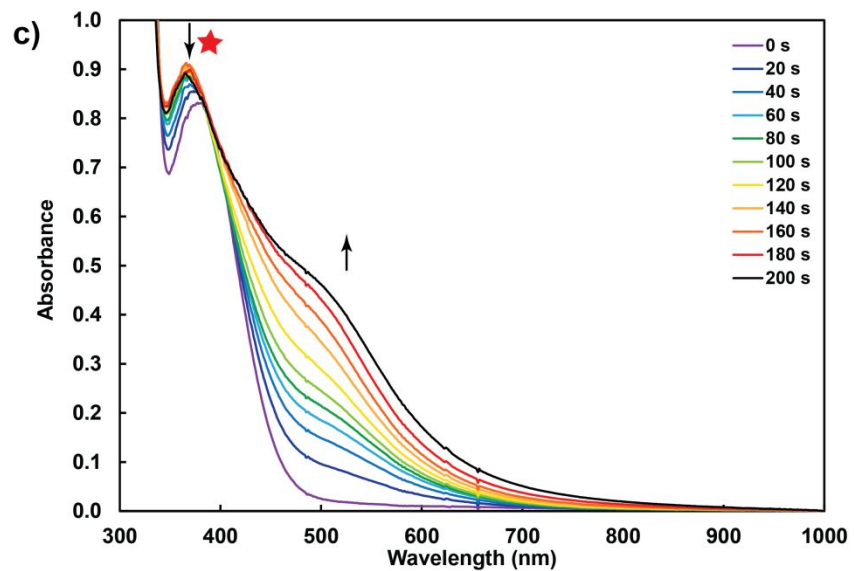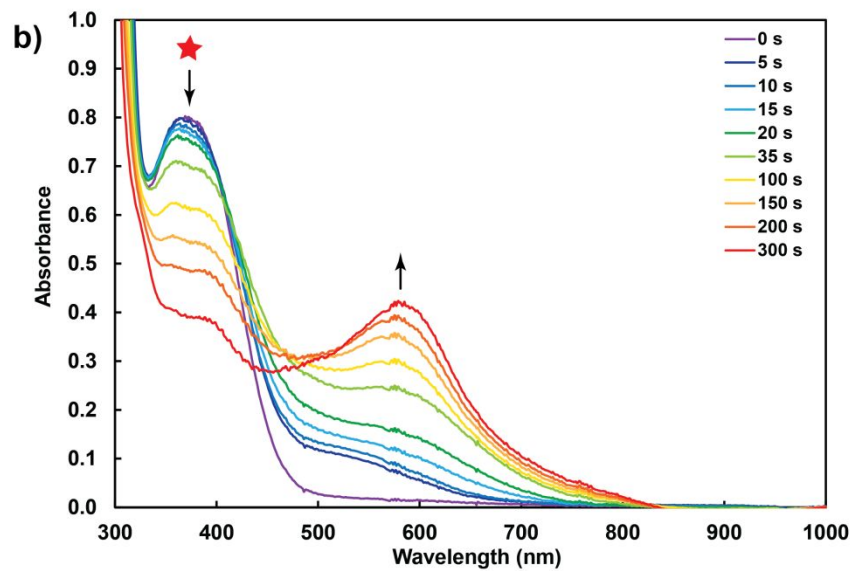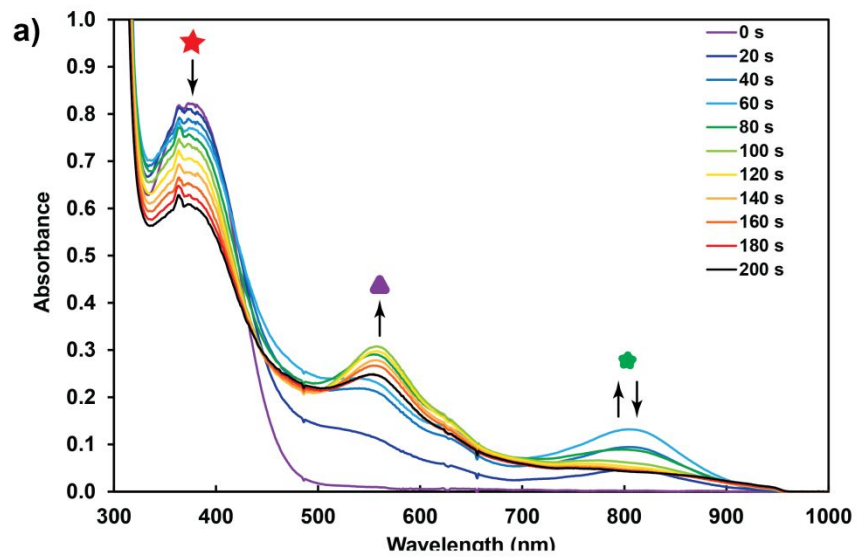**Figure 5**. [Mn(bpy)(CO)2(MeCN)(CN)], abbreviated **s-MnCN**.

Figure 6. UV-vis absorption spectra changes of a) **MnCN**, b) **MnCN** with tetrabutylammonium cyanide (TBACN), and c) **MnCN(mesbpy)** at 298 K upon irradiated with a 395 nm LED (2.97 × 10^{-9} einstein per s intensity). MnCN is indicated by ⭐, [Mn(bpy)(CO)$_3$]$_2$ by ⭐, and [Mn(bpy)(CO)$_3$]⁻ by ▲.

The **s-MnCN** species located in the UV-vis spectra (**Figure 6**) at ~530 nm appears within the first seconds of irradiation. Upon further irradiation, features indicative of [Mn(bpy)(CO)$_3$]$_2$ increase at 20 s and subsequently decrease at 60 s, indicated by the peak at 806 nm in Figure 6a.[45] This suggests that [Mn(bpy)(CO)$_3$]$_2$ is an intermediate and is consumed in the reaction. Perhaps most interesting is the formation of [Mn(bpy)(CO)$_3$]⁻, the proposed active species in CO$_2$ reduction. [Mn(bpy)(CO)$_3$]⁻ is observed after 20 s of irradiation with an MLCT band at 569 nm.[33] Based upon this analysis, the following reaction mechanism is proposed for the photochemical formation of the [Mn(bpy)(CO)$_3$]⁻ anion from **MnCN**.
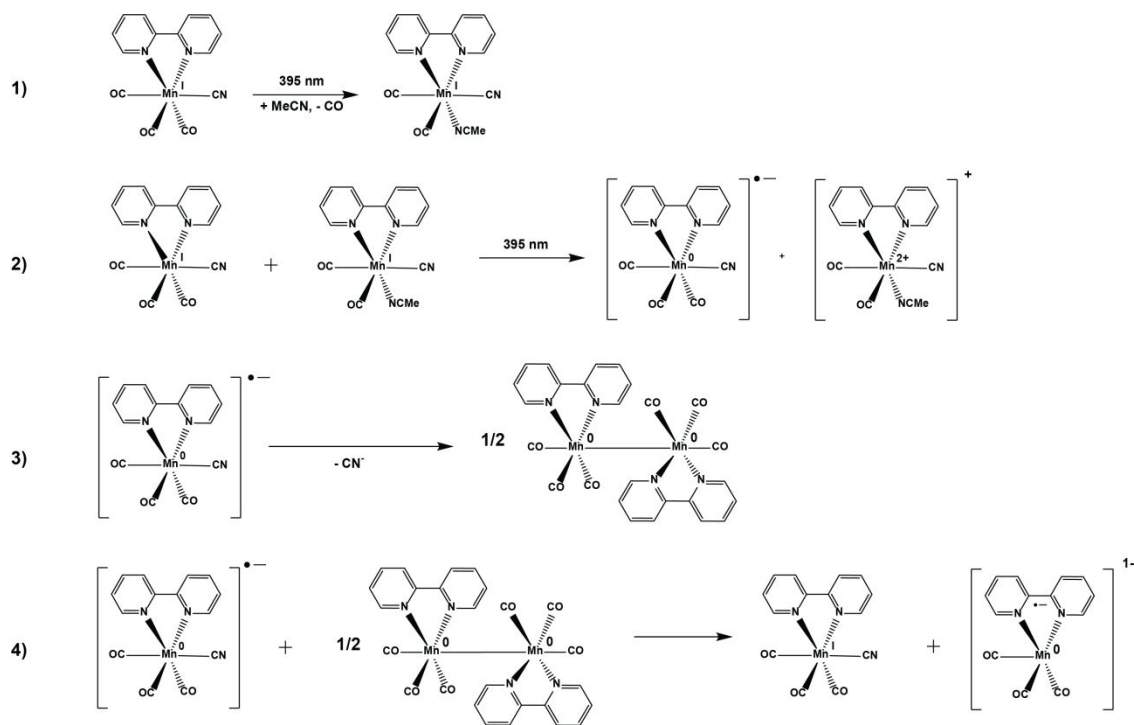

Figure 7. Proposed stoichiometric reaction mechanism for the photochemical formation of [Mn(bpy)(CO)$_3$]⁻ from **MnCN**.

10

To determine whether or not step (2) in **Figure 7** is a photochemical transformation, **s-MnCN** was first synthesized by irradiating **MnCN** in MeCN in the presence of oxygen, to prevent further reactivity.[36] The solvent was stripped off this reaction and the product was redissolved in thoroughly degassed and dry MeCN. Separate experiments were then carried out on a mixture of **s-MnCN** and the starting material, **MnCN**: a dark control, irradiation at 517 nm, and irradiation at 395 nm. Illumination at 517 nm is only absorbed by **s-MnCN**, and 395 nm is absorbed selectively by **MnCN**. There was no reaction in the dark after 1 hour, or when the 517 nm light was used (**Figure S8**). The reaction only proceeded when the mixture was irradiated at 395 nm. This suggests that there is an electron-transfer where **s-MnCN** acts as a sacrificial reductant to the excited [**MnCN**]* by giving one electron, affording the radical anion. Similar behavior was previously observed with s-Mn$_2$CN$^+$ under irradiation.[36]

The radical anion, after loss of the cyano ligand, can undergo dimerization to form [Mn(bpy)(CO)$_3$]$_2$ as an intermediate.[42] Further reaction of the dimer with the singly reduced [Mn(bpy)(CO)$_3$CN]$^{\bullet-}$ species leads to the formation of both [Mn(bpy)(CO)$_3$]$^-$ and **MnCN**. An important observation is that under aerobic conditions, neither [Mn(bpy)(CO)$_3$]$^-$ nor [Mn(bpy)(CO)$_3$]$_2$ formed, as spectroscopically reported in **Figure S5**.

From the point of view of CO$_2$ photocatalysis, it is desirable to form [Mn(bpy)(CO)$_3$]$^-$ without the formation of the dimeric [Mn(bpy)(CO)$_3$]$_2$ byproduct.[20] It has previously been shown that incorporation of the bulky mesbpy ligand prevents dimerization under electrochemical conditions.[28] Photochemically, the bulkiness of **MnCN(mesbpy)** served to shut down reactivity beyond **s-MnCN(mesbpy)** formation (**Figure 6c** and **Figure S9**). Interestingly, the terminal-CN$^-$ ligand remained intact upon irradiation, unlike the axial Br$^-$ ligand in **MnBr(mesbpy)** which

dissociated, leaving behind a bis-acetonitrile species (**Figure S10**). The lack of further

photochemical transformations by **MnCN(mesbpy)** is attributed to its inability to dimerize - step

(3) in **Figure 7**.

      To test for the existence of step (3), tetrabutylammonium cyanide (TBACN) was added to

the reaction. The addition of TBACN was expected to aid in the recovery of the cyano complex

after the loss of cyanide from the radical anion. Noted by the absence of a UV-vis absorption

peak at 806 nm (**Figure 6b**), the addition of TBACN to a solution of MnCN did prevent the

formation of $[Mn(bpy)(CO)_3]_2$. Upon irradiation, the yellow solution turned grey-purple, not the

vibrant purple of $[Mn(bpy)(CO)_3]^-$. The UV-vis showed an MLCT band that was slightly red-

shifted from $[Mn(bpy)(CO)_3]^-$ at 572 nm, and lacked the shoulder at 640 nm characteristic of
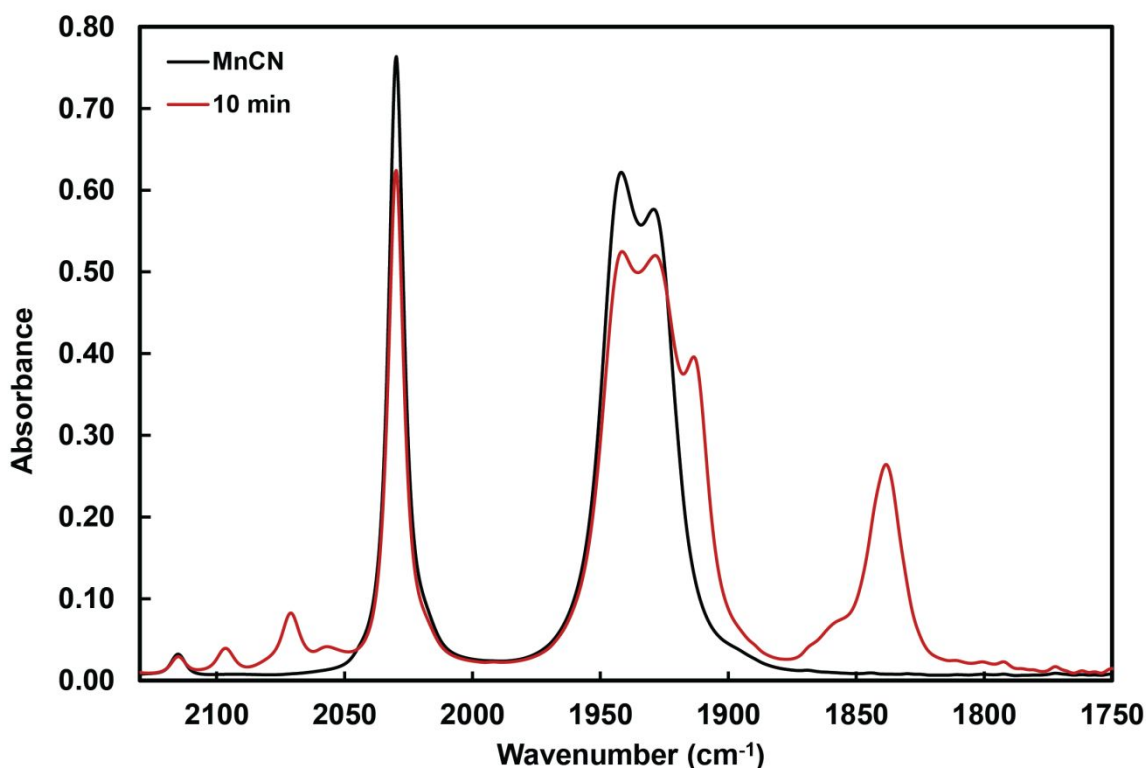
$[Mn(bpy)(CO)_3]^-$.

Figure 8. Liquid phase IR spectra of MnCN (black) and a solution of **MnCN** with 4 equivalents
of TBACN after 10 min of irradiation at 395 nm at 2.97×10^{-9} einstein per s intensity (red).

The liquid phase IR spectrum shown in **Figure 8** supports this interpretation of **Figure 6b**, revealing that neither [Mn(bpy)(CO)$_3$]$_2$ (1978, 1932, 1882, and 1863 cm^{-1})[46] nor [Mn(bpy)(CO)$_3$]$^-$ (1916 and 1814 cm^{-1})[47] are present in solution. Rather, there are two terminal cyanide peaks located at 2070 and 2054 cm^{-1}, as well as two carbonyl peaks at 1911 and 1837 cm^{-1}, suggesting the presence of a bis-cyano species, [Mn(bpy)(CO)$_2$(CN)$_2$]$^-$. The peak at 2115 cm^{-1} belongs to the CN-ligand of the **MnCN** starting material and the CN-peak at 2094 cm^{-1} is associated with the formation of HCN.[48] The shoulder at 1860 cm^{-1} is assigned to a small amount of the **s-MnCN** species. This biscyano species, has a *cis*-dicarbonyl structure based on the 1911 and 1837 cm^{-1} peak pattern.[49] Unlike **s-MnCN**, where an equatorial carbonyl is substituted by an acetonitrile solvent ligand, a CN$^-$ replaces an axial carbonyl in this case. The *trans*-biscyano structure shown in **Figure 9a** is supported by DFT calculations over the CN$_{ax}$, CN$_{eq}$ structure, as it is 1.2 kJ/mol more stable. The additional cyanide ligand changes the overall charge of the complex to -1, which is consistent with the observed red-shifted carbonyl IR stretches.
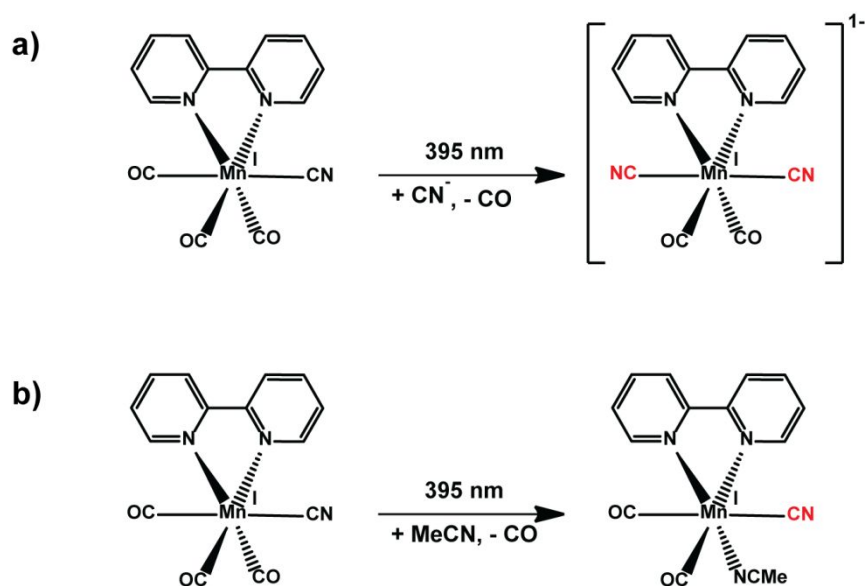

Figure 9. Scheme of two photochemical reactions of MnCN where a carbonyl ligand, rather than a CN$^-$ ligand is the leaving group.

Previously reported electrochemical data indicates that reducing **MnBr** by two electrons

produces [Mn(bpy)(CO)$_3$]$^-$, the proposed active species for CO$_2$ reduction.[20, 47] As

[Mn(bpy)(CO)$_3$]$^-$ was photochemically produced by **MnCN** alone, the ground state reduction

chemistry of **MnCN** was explored using Na(Hg) as the reducing agent.
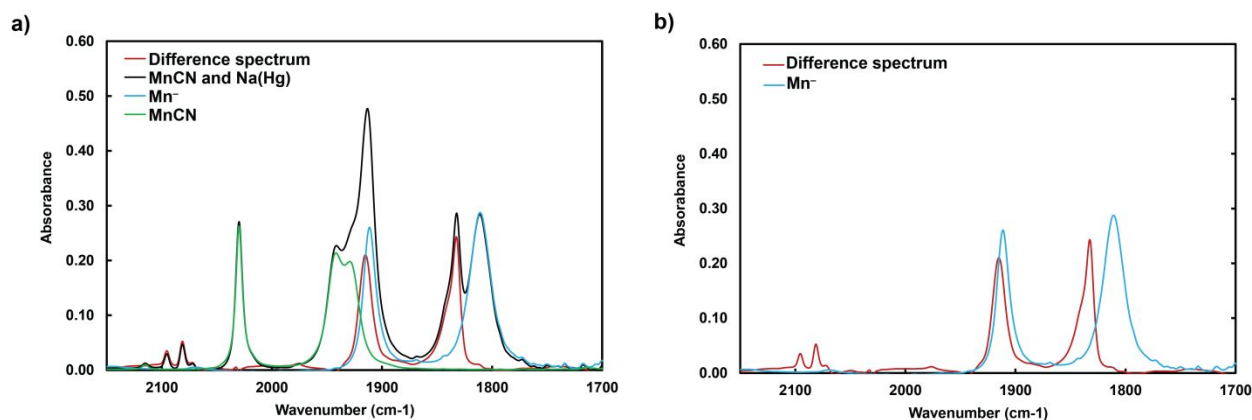
Figure 10. The liquid phase IR spectrum of **MnCN** with 1 eq. Na(Hg) (black), showing the constituent species that contribute to the overall signal. The difference spectrum (red) was obtained by fitting the unique axial carbonyl peak at 2029 cm^{-1} to **MnCN** and the unique peak at 1811 cm^{-1} for [Mn(bpy)(CO)$_3$]$^-$.

The liquid phase IR spectrum (black trace) contains a mixture of different manganese

species (**Figure 10**). The IR stretches of the doubly reduced species, [Mn(bpy)(CO)$_3$]$^-$, are well

known in MeCN at 1911 and 1811 cm^{-1}, indicating that another species besides starting material

was present and responsible for the 1830 cm^{-1} peak. By subtracting the peak components

belonging to **MnCN** and [Mn(bpy)(CO)$_3$]$^-$, a difference spectrum in red was revealed. This

additional species has a terminal cyanide peak at 2081 cm^{-1} as well as two carbonyl peaks in a

classic CO$_{ax}$, CO$_{eq}$ pattern (1911 and 1830 cm^{-1}).[43] The peak at 2094 cm^{-1} belongs to HCN.[48]

Based upon this IR spectrum, there exists an alternate reaction pathway for **MnCN** when it is

chemically reduced, whereby the CN-ligand is retained (**Figure 11**).
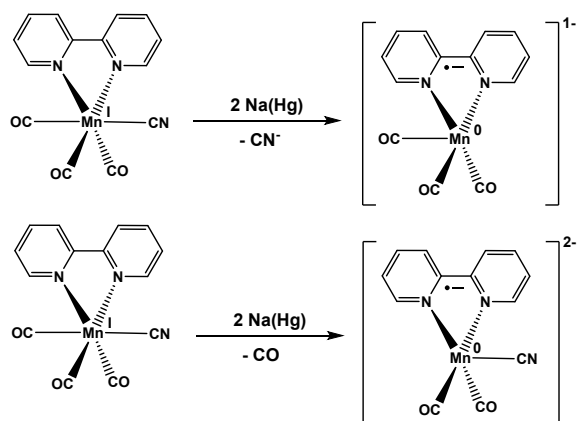
Figure 11. Schematic summarizing the results of reducing **MnCN** using 1 eq. of Na(Hg), a chemical reductant.
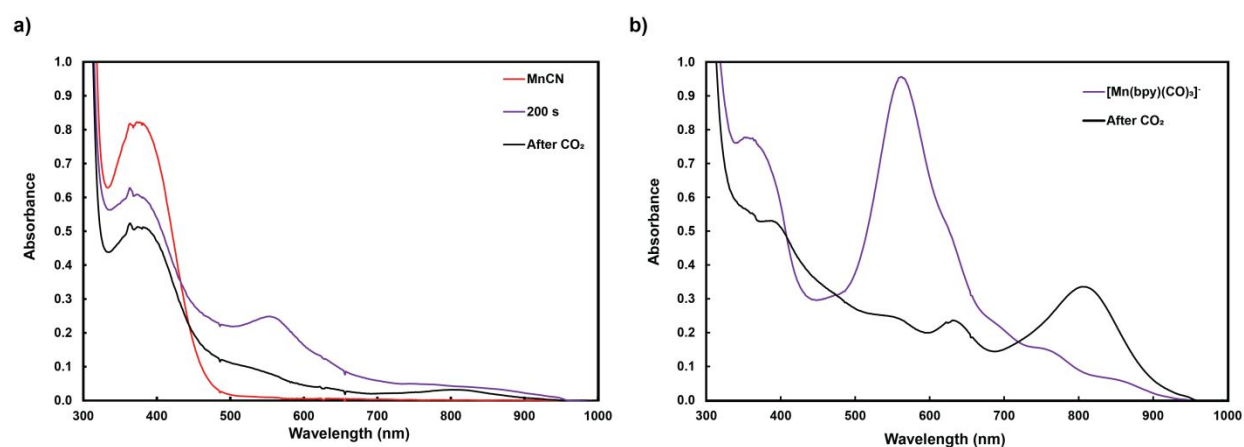
Figure 12. UV-vis of a) 0.2 mM MnCN before and after 200 s of irradiation at 395 nm (2.97×10^{-9} einstein per s intensity), and then upon exposure to CO_2 post-irradiation and b) 0.069 mM of [Mn(bpy)(CO)$_3$]$^-$ before and after exposure to CO_2 in dry MeCN.

Since the anion, [Mn(bpy)(CO)$_3$]$^-$, is the active species for CO_2 reduction, the anion generated by irradiating MnCN at 395 nm was allowed to react with CO_2. As seen in **Figure 12**, after 200 s of irradiating MnCN into the MLCT band using a 395 nm LED, [Mn(bpy)(CO)$_3$]$^-$ is formed at 569 nm.[33] After exposure to CO_2, however, the dimeric species, [Mn(bpy)(CO)$_3$]$_2$ is formed at 805 nm.[33] Consistent with these findings is the observation that a pristine 0.069 mM

sample of [Mn(bpy)(CO)$_3$]$^-$, synthesized by adding two equivalents of Na(Hg) to **MnBr**, forms

0.028 mM [Mn(bpy)(CO)$_3$]$_2$ upon exposure to CO_2, with the color changing from deep purple to

olive green. It has been previously reported that [Mn(CO)$_3$(bpy)]$_2$ can be synthesized by adding a

starting Mn^I species, such as **MnBr**, to one equivalent of the anionic species, [Mn(CO)$_3$(bpy)]$^-$.[46]

As shown in **Scheme 1**, the anionic species first reduces CO_2 by two electrons, using trace water

found in MeCN, forming a Mn^I species that then rapidly reacts with remaining anion in solution,

resulting in the observed dimer.[50]
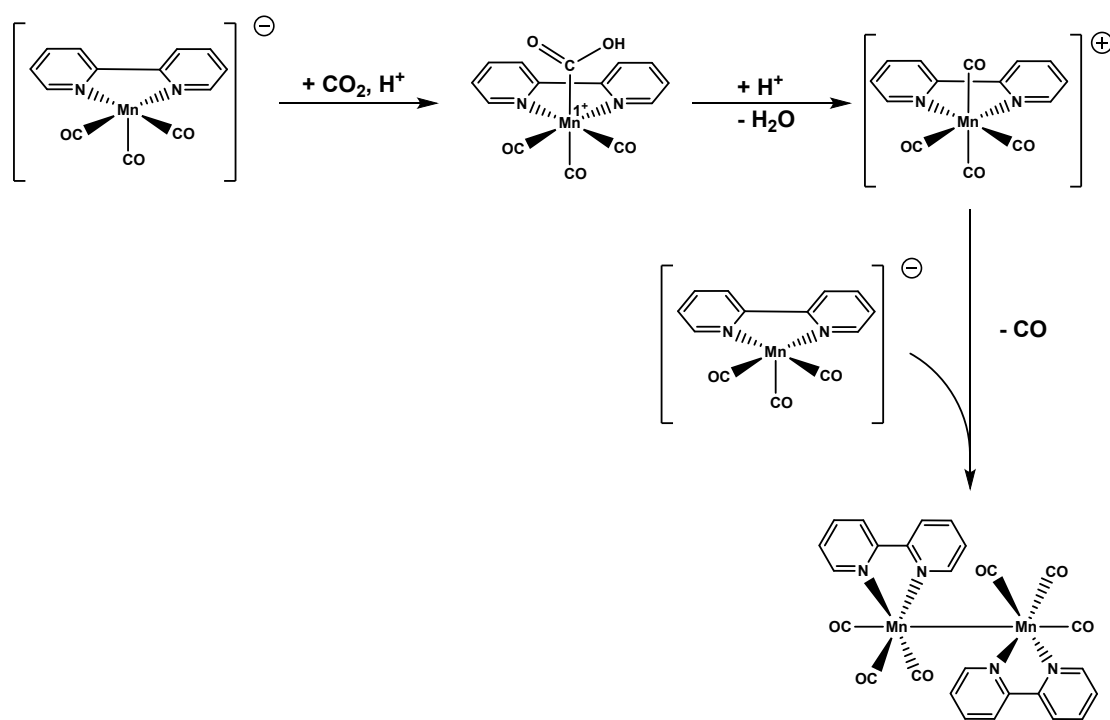
Scheme 1. Schematic showing the formation of the Mn-Mn dimer from [Mn(CO)$_3$(bpy)]$^-$ reacting with a Mn^I species.

Photochemical CO$_2$ Reduction

To ascertain that CO found in the reaction headspace is from CO_2 photoreduction and not simply

carbonyl ligand dissociation, we utilized $^{13}CO_2$. A total of 35.4 micromoles of CO were detected

in the headspace via GC analysis, which equates to a total quantum yield for CO production of

0.55. From the gas phase IR spectrum of the reaction products shown in **Figure 13**, only 6.1% of

the total CO produced is ^{13}CO. Using this percentage of ^{13}CO, the value of the quantum yield for

the formation of CO from CO_2 is only 0.033. Still, it is important to note that without the use of

an additional photosensitizer, **MnCN** is able to form the active species, [Mn(bpy)(CO)$_3$]$^-$, and

reduce CO_2 to CO using light.
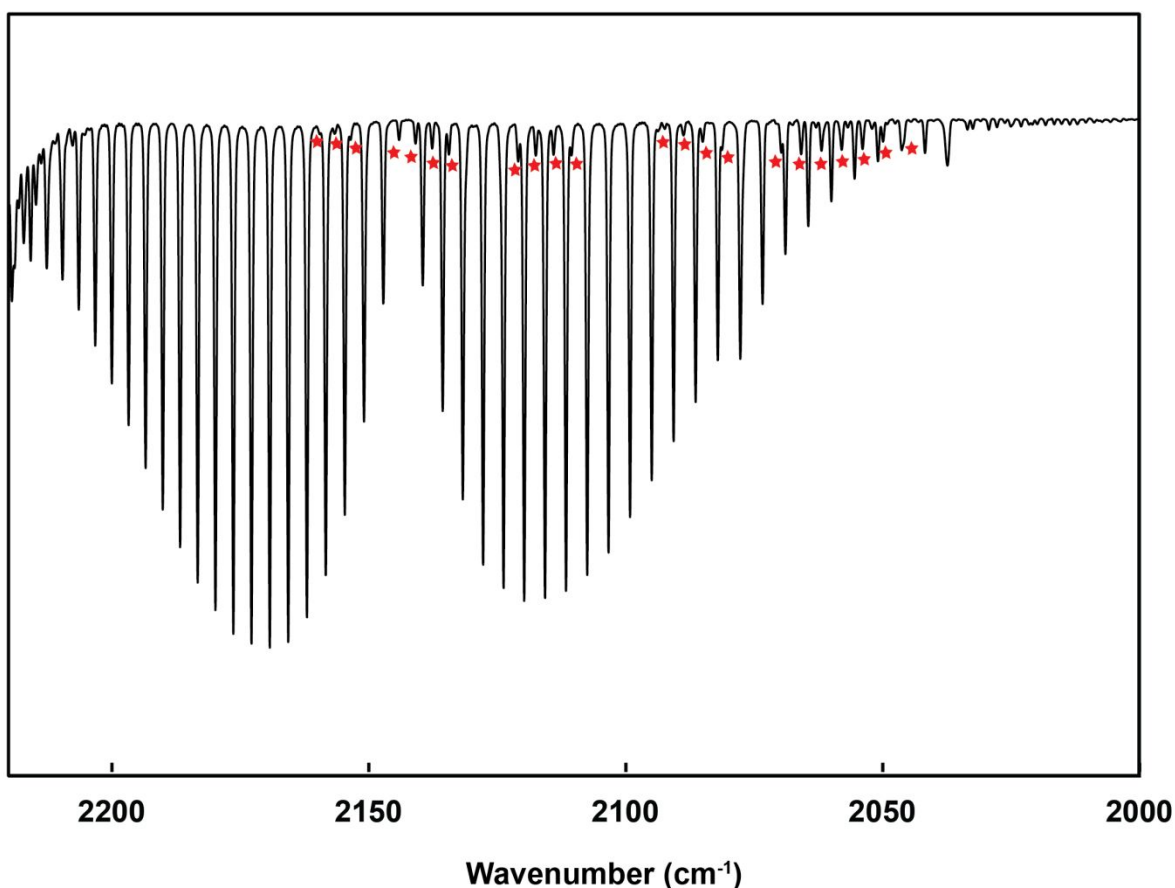
Figure 13. Gas phase IR spectrum of a photolysis experiment with 1 mM MnCN, 0.5 M PhOH, in 8 mL $^{13}CO_2$-saturated MeCN, after irradiation for 1 hour with a 395 nm LED, with an intensity of 1.81 x 10^{-8} einstein per second. The headspace sample contains both ^{12}CO and ^{13}CO (red stars). The vibrotor transitions for ^{12}CO are centered at 2140 cm^{-1}, whereas the ^{13}CO transitions are centered at 2100 cm^{-1}.

17

Table 2. Quantum yield (Φ) of CO produced by 1 mM MnCN in CO_2-saturated MeCN with 0.5 M PhOH over time compared with the corrected quantum yield using the ratio of ^{13}CO to total CO found in the gas phase IR experiment (6.1%).

Irradiation time (min) at 395 nm	Light In (mW)	Light Out (mW)	Photons absorbed (x 10^{-5})	CO (μmol)	Φ_{CO}[1]	Corrected Φ_{CO}
0	5.480	0.030	0	0	0	0
10	5.480	0.111	1.064	15.4	1.45	0.088
20	5.480	0.425	2.004	21.2	1.06	0.065
30	5.480	0.433	3.001	27.9	0.93	0.057
40	5.480	0.438	3.998	28.4	0.71	0.043
50	5.480	0.438	4.997	29.3	0.59	0.036
60	5.480	0.438	5.997	30.5	0.51	0.031

[1]Quantum yield was calculated by dividing mol of CO produced by the Einsteins of the photons absorbed.

Although rarely noted in the literature for this class of complexes, it is important to take into account the simultaneous photodegradation of $[Mn(N-N)(CO)_3X]$ complexes when discussing their CO_2 photoreduction capabilities, as this accounts for a significant amount of the evolved CO observed. As seen in **Table 2**, the amount of light that is transmitted by a sample of 1 mM **MnCN**, denoted "Light Out," increases as irradiation time increases. This is because of the photodegradation of **MnCN** that also leads to quantum yields >1 at early time points. Quantum yields greater than unity are an artifact due to the co-generation of CO from CO_2 photoreduction and complex degradation and should be taken with caution as they are not a true reflection of the CO_2 photoreduction proficiencies of **MnCN**. We demonstrate here the importance of utilizing $^{13}CO_2$ in understanding the actual CO_2 reducing power of these complexes.

Electrochemistry

The cyclic voltammograms of relevant Mn complexes are shown in **Figure 14**. Notably, the cyclic voltammogram of **MnCN(mesbpy)** more closely resembles that of **MnCN**, rather than

MnBr(mesbpy). Both complexes with **mesbpy** ligands lack the oxidation peak which has been

attributed to the oxidation of a Mn-Mn dimeric species (-0.61 V vs. Fc/Fc$^+$). This is attributed to

the steric bulk of the monomeric species. However, **MnCN(mesbpy)** features two, one-electron

reductions like **MnCN**, while **MnBr(mesbpy)** has a single two-electron reduction feature.[28]
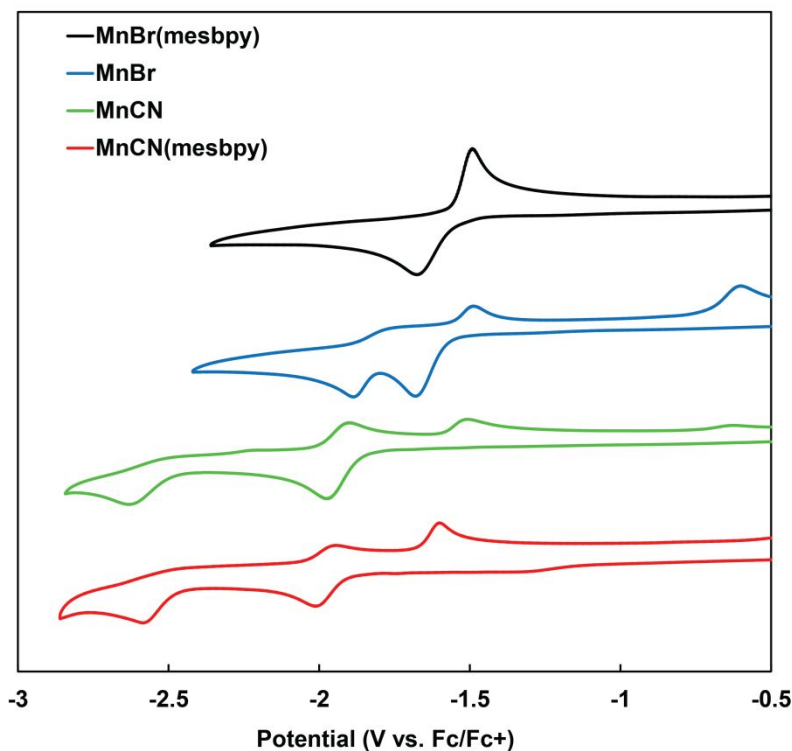
Figure 14. Comparison of cyclic voltammograms of relevant Mn complexes at 250 mV/s in dry, degassed MeCN at 298 K.

By comparison with **MnCN**, the first reduction feature at -1.98 V vs. Fc/Fc$^+$ is assigned

to a one-electron reduction of **MnCN(mesbpy)** to the anionic radical species

[Mn(mesbpy)(CO)$_3$CN]$^{\bullet-}$. The second reduction at -2.56 V vs. Fc/Fc$^+$ is associated with the

formation of the anionic active species for CO$_2$ reduction, [Mn(mesbpy)(CO)$_3$]$^-$, followed by the

loss of CN$^-$.

As seen in **Figure 15**, when the switching potential is set just after the first reduction

event, only the first reduction and first oxidation peaks are present, revealing that they are

coupled, consistent with the bpy version of the Mn complex. When the switching potential is at -2.9 V vs. Fc/Fc$^+$, the second reduction event and the second oxidation event are observed. The second oxidation event at -1.55 V vs. Fc/Fc$^+$ belongs to the two-electron oxidation of the doubly reduced [Mn(mesbpy)(CO)$_3$]$^-$, to the neutral radical, then to [Mn(mesbpy)(CO)$_3$]$^+$. The [Mn(mesbpy)(CO)$_3$]$^+$ species is then captured by free CN$^-$ to reform the initial complex.
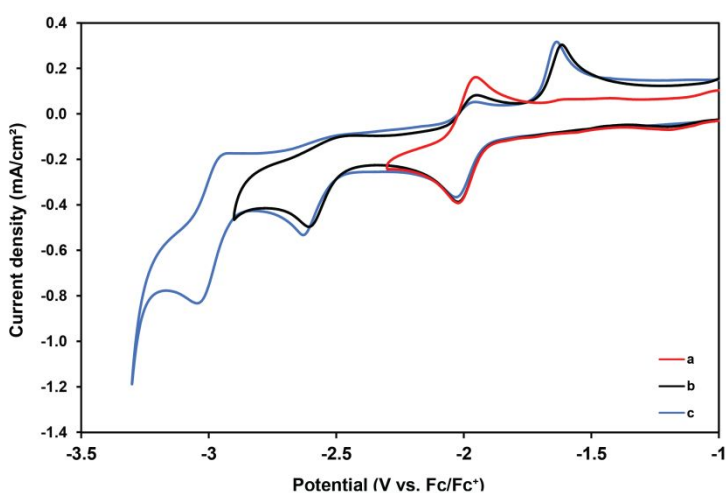
Figure 15. Cyclic voltammograms of **MnCN(mesbpy)** at 250 mV/s in dry, degassed MeCN with 0.1 M TBAPF$_6$ supporting electrolyte. The switching potentials are A: -2.3, B: -2.9, and C: -3.3 V vs. Fc/Fc$^+$.

This is similar to the electrochemical behavior of MnBr(mesbpy) reported by Kubiak *et al.*, where there is a two-electron oxidation of [Mn(mesbpy)(CO)$_3$]$^-$ at *ca.* 1.5 V vs. Fc/Fc$^+$.[28] The

$$Mn^ICN(mesbpy) + e^- \rightarrow [Mn^ICN(mesbpy^{\bullet-})]^- \ (E_{1/2} = -1.98 \ V)$$
$$[Mn^ICN(mesbpy^{\bullet-})]^- + e^- \rightarrow [Mn^0CN(mesbpy^{\bullet-})]^{2-} \ (E_{1/2} = -2.56 \ V)$$
$$[Mn^0CN(mesbpy^{\bullet-})]^{2-} \rightarrow [Mn^0(mesbpy^{\bullet-})]^- + CN^-$$
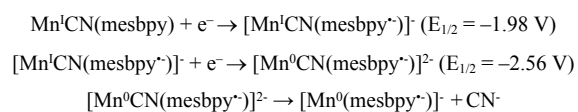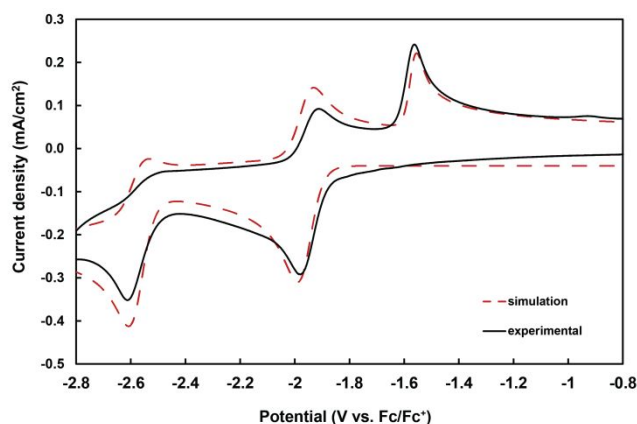
following EEC mechanism is supported by digital cyclic voltammetry simulation using DigiElch 4.0 as seen in **Figure 16**.

Figure 16. Comparison of experimental and simulated cyclic voltammograms at 250 mV/s of 1 mM **[Mn(mesbpy)(CO)$_3$(CN)]** in dry, degassed MeCN with 0.1 M TBAPF$_6$ under Ar. The value of the working electrode area (0.071 cm^2) and the scan rate were imported into the simulated CV.
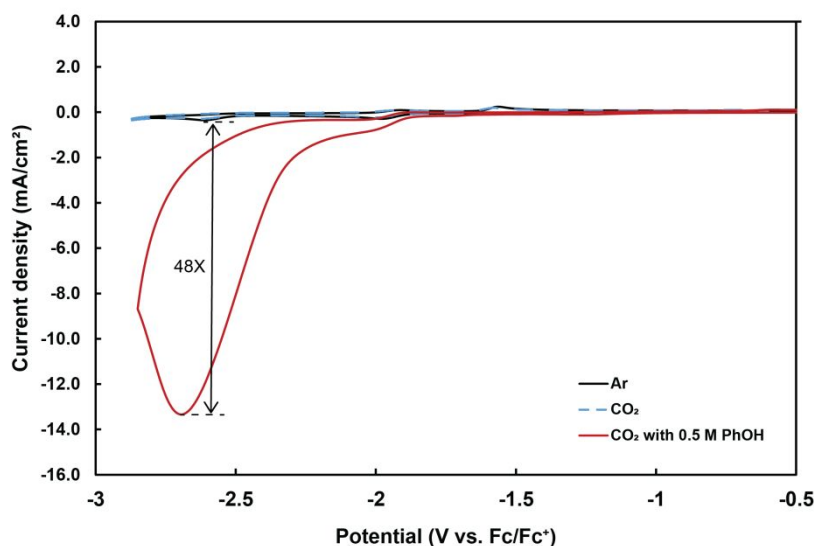
Figure 17. Cyclic voltammetry data of 1 mM **MnCN(mesbpy)** under argon, under CO$_2$, and under CO$_2$ with 0.5 M PhOH at a scan rate of 250 mV s^{-1}. Current enhancement of 48x is shown at the second reduction potential at -2.56 V. vs Fc/Fc$^+$.

Cyclic voltammetry was also used to probe the CO_2 electroreduction capability of

MnCN(mesbpy). As displayed in **Figure 17 (black curve)**, no significant change in the

voltammogram is observed upon the addition of CO_2, except for a slight shift in the second

reduction peak from -2.56 to -2.64 V vs. Fc/Fc^+. It is known that $[Mn(N-N)(CO)_3X]$ complexes

require a proton source to reduce carbon dioxide to carbon monoxide.[20] Upon addition of 0.5 M

phenol as the proton source, a 48 times current enhancement is seen at the second reduction

potential of **MnCN(mesbpy)** and the oxidative peak at -1.5 V vs. Fc/Fc^+ disappears. This is

consistent with the observation that $[Mn(mesbpy)(CO)_3]^-$ is the active species for CO_2 reduction.

To further explore this electrocatalytic transformation, 1 mM of **MnCN(mesbpy)** in CO_2

saturated, wet MeCN was held at the second reduction potential for 4 h. The gaseous products

were identified using headspace gas chromatographic analysis. Using 0.5 M phenol as the proton

source resulted in a faradaic efficiency (ξ_{CO}) of 88% for CO production (65.7 μmol CO). ^1H

NMR analysis of a post-electrolysis solution showed no formate was produced (**Figure S15**).

Figure 18. Gas phase IR spectrum of a 3-hour bulk electrolysis at the second reduction potential of MnCN(mesbpy), with 1 mM MnCN(mesbpy), 0.5 M PhOH, in 20 mL $^{13}CO_2$-saturated MeCN. The signals for ^{12}CO (blue) and ^{13}CO (red) overlap (purple) in the range from 2060 to 2175 cm^{-1}.
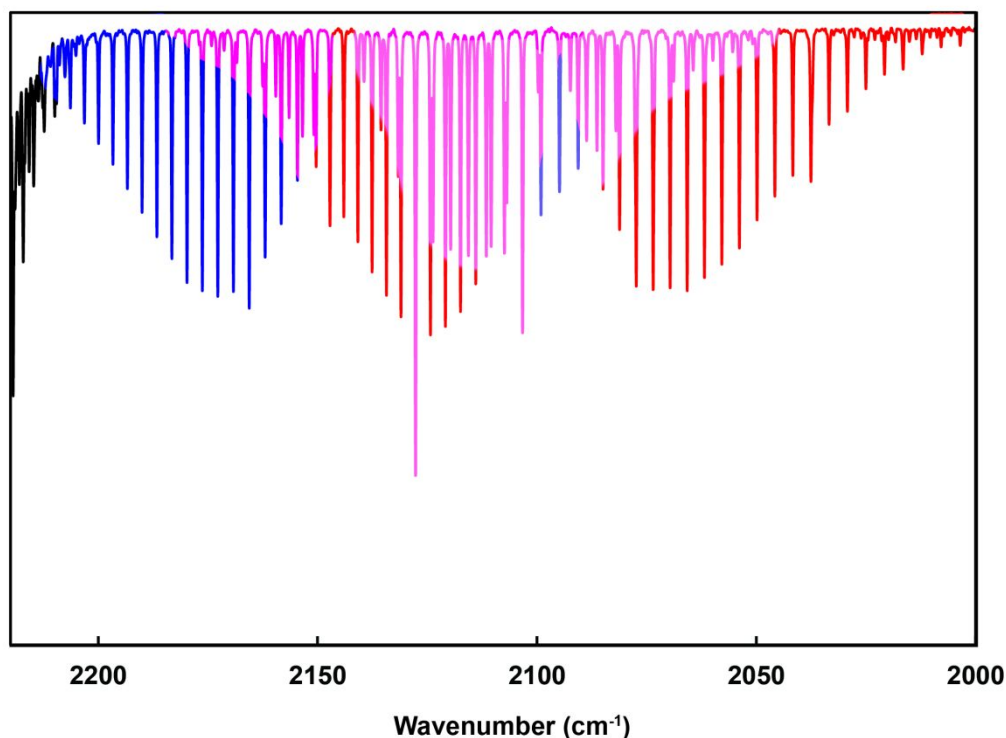
An isotopic labeling experiment using $^{13}CO_2$ was performed to ensure that the carbon monoxide produced originated from carbon dioxide electroreduction. After a three-hour electrolysis experiment, the headspace gas was analyzed by IR (**Figure 18)**, and found to consist of a mixture of ^{13}CO (46%) and ^{12}CO (54%). The presence of both isotope labels is expected mechanistically as all CO ligands are kinetically equivalent. Typically a 1:3 ratio of ^{13}CO:^{12}CO is observed, originating from a $[Mn(bpy)(^{13}CO)(^{12}CO)_3]^+$ intermediate.[25, 26, 38, 39] For **MnCN(mesbpy)**, the elongated bond lengths in the axial directions might favor the dissociation of the axial carbonyl ligands, leading to a 1:1 ratio of ^{13}CO:^{12}CO.

Conclusion

The photochemistry of **MnCN** was explored without an additional photosensitizer and found to be active for photochemical CO_2 to CO conversion. A photochemical mechanism was proposed and supported by the inability of the bulky **MnCN(mesbpy)** to undergo the same reaction steps. **MnCN** was successfully able to specifically form $[Mn(bpy)(CO)_3]^-$ under irradiation into its MLCT transition. In contrast, reducing **MnCN** with two equivalents of Na(Hg) produced a mixture of $[Mn(bpy)(CO)_3]^-$ and $[Mn(bpy)(CO)_2(CN)]^-$, demonstrating a difference in the ground state versus excited state charge transfer chemistry. Additional photolysis experiments with TBACN revealed that a cis-dicyano-dicarbonyl complex results, preventing formation of the dimer. We demonstrate the importance of studying these complexes photochemically in the presence of $^{13}CO_2$, as artificially high quantum yields can result when photodegradation is not considered. Electrocatalytically, **MnCN(mesbpy)** was found to reduce CO_2 to CO without dimer

formation. Unlike for **MnBr(mesbpy)**, where the first two reduction events occur at the same potential due to the bulky mesbpy ligand, cyano ligand retention was more influential in determining the potential of the second reduction of **MnCN(mesbpy)**. Overall, axial-cyano ligands confer unusual reactivity for this class of manganese complexes.

Photochemically, the active CO_2 reduction complex, $[Mn(mesbpy)(CO)_3]^-$, was unable to form

due to the steric bulk of the mesbpy ligand preventing the dimerization reaction needed to form this species. However, electrochemically, the working electrode was able to deliver electrons to **MnCN(mesbpy)**, forming the catalytically active species. In this case, the steric bulk was beneficial in shutting down dimer formation, but didn't interfere with the electrochemical reduction process.

Experimental Section

General Procedures

For electrochemical experiments, the electrolyte was bubbled with either Ar or CO_2 for 20 min before measuring a background scan. The electrolyte was bubbled for an additional 10 min after adding the desired complex. 1 mM of the Mn complex and 0.1 M TBAPF$_6$ supporting electrolyte were added for both bulk electrolysis and cyclic voltammetry experiments. Ag/AgCl or Ag/AgNO$_3$ (10 mM) was used as the reference electrode and ferrocene was added as an internal reference. The total volume of the solution for CV and bulk electrolysis was 20 mL. $[Mn(bpy)(CO)_3]^-$ was synthesized by adding two equivalents of Na(Hg) to a MeCN solution of **MnBr** under argon. The solution was then filtered through a plug of celite.

Materials

The complex, **MnCN**, was synthesized following a literature procedure, where [Mn(bpy)(CO)$_3$Br] was added to AgCN and allowed to reflux for 1.5 h.[38] For **MnCN(mesbpy)**, the ligand 6,6′-dimesityl-2,2′-bipyridine (**mesbpy**) was first synthesized according to a previous report.[28] **Mesbpy** was synthesized in a three-day Suzuki coupling reaction using 6,6'-dibromo-2,2'-bipyridine and 2,4,6-trimethylphenylboronic acid. The resultant **mesbpy** ligand was characterized using ATR-IR and found to match previous literature reports.[51] A 2 h reflux reaction between Mn(CO)$_5$Br and mesbpy yielded [Mn(mesbpy)(CO)$_3$Br], abbreviated **MnBr(mesbpy)**. The addition of AgCN to **MnBr(mesbpy)** gave **MnCN(mesbpy)** after a 24 h reflux in methanol with a yield of 75%.

All reagents were purchased from commercial supplies and used without additional purification. Anhydrous MeCN was purchased from Sigma-Aldrich (sure/seal), degassed using the freeze-pump-thaw method, and stored over 3 Å molecular sieves. MeCN was stored under Ar in the glovebox and dried again over a column of activated alumina before use. Tetrabutylammonium hexafluorophosphate (TBAPF$_6$, Sigma-Aldrich) and tetrabutylammonium cyanide (TBACN, Sigma-Aldrich) were stored in the glovebox. Manganese complexes were handled in the dark. **MnCN** and **mesbpy** were synthesized according to literature procedures.[28, 38] A 3 mm glassy carbon working electrode, a Pt wire fitted with a Pt mesh (~0.5 cm^2) counter electrode, and either a Ag/AgCl or Ag/AgNO$_3$ (10 mM) reference electrode was used in all electrochemical experiments. A four-neck flask was used for CV and bulk electrolysis.

Instrumentation

CV and bulk electrolysis experiments were performed on CHI 760D electrochemical workstation (CH Instruments, Austin, TX). Gas and liquid phase FT-IR spectra were measured on a Nicolet Model 730 FT-IR spectrometer. UV-vis spectra were measured using a Cary 60 UV-vis spectrophotometer (Agilent Technologies). Gaseous products were detected using a 3 min isotherm at 80 $^\circ$C using an SRI 8610C Gas Chromatograph and TCD. Headspace gas was analyzed via gas-phase IR in a cell fitted with CaF_2 plates. NMR spectra were recorded on a 500 MHz Bruker Avance-III NMR instrument equipped with a cryoprobe. All digital cyclic voltammetric simulations were performed using DigiElch 4.0.

Photochemical Reactions

In photolysis studies, 8 mL MeCN with 0.5 M PhOH and 1 mM **MnCN** was added to a clear borosilicate glass vial with a septum cap. The vial was irradiated at 395 nm with an LED light under stirring. The headspace was sampled via GC or in a gas cell terminated with KBr plates. In UV-vis studies, a 1-cm pathlength quartz cuvette (Starna) fitted with a screw cap was used. For the liquid phase IR studies, 5 mM of the Mn sample in MeCN was loaded in a demountable liquid cell terminated with CaF_2 windows in the glove box.

Computational Methodology. Gaussian 16[52] via Density Functional Theory (DFT) with the M06[53] functional level of theory and 6-311G** basis set[54] were used to perform geometry optimization of the ground-state of molecules of interest. LANL2DZ[55] basis set was applied on the manganese metal center which describes inner electrons of the metal with effective core potentials. Polarizable Continuum Model (PCM)[56] with acetonitrile was utilized to mimic

experimental conditions. Frequencies were calculated to confirm no imaginary frequencies and in order to obtain the IR spectrum.

Preparation of Mn(mesbpy)(CO)₃CN. Mn(mesbpy)(CO)₃Br (0.92 g, 1.5 mmol) and AgCN (0.22 g, 1.64 mmol) were added to a Schlenk flask with 50 mL methanol, and refluxed under Ar with constant stirring in the dark for 24 hours. The solution was then filtered through celite and the filtrate collected via rotary evaporation. The complex was recrystallized as an orange-yellow solid in CH_2Cl_2 layered with diethyl ether (0.63 g, 75%). ^1H NMR (400 MHz, CD_3CN): $\delta = 2.04$ (s, 12H, CH_3), 2.32 (s, 6H, CH_3), 7.01 (s, 4H, phenyl H), 7.41 (d, 2H, 5,5′ H, J = 8 Hz), 8.15 (m, 2H, 4,4′ H, J = 8 Hz), 8.43 (d, 2H, 3,3′ H, J = 8 Hz). IR (cm⁻¹) ν_{CN}: 2115, ν_{CO}: 2022, 1930.

Conflicts of interest

There are no conflicts to declare.

Acknowledgements

References

1.   Sherwood, S. C.; Webb, M. J.; Annan, J. D.; Armour, K. C.; Forster, P. M.; Hargreaves, J. C.; Hegerl, G.; Klein, S. A.; Marvel, K. D.; Rohling, E. J.; Watanabe, M.; Andrews, T.; Braconnot, P.; Bretherton, C. S.; Foster, G. L.; Hausfather, Z.; von der Heydt, A. S.; Knutti, R.; Mauritsen, T.; Norris, J. R.; Proistosescu, C.; Rugenstein, M.; Schmidt, G. A.; Tokarska, K. B.; Zelinka, M. D., An Assessment of Earth's Climate Sensitivity Using Multiple Lines of Evidence. *Reviews of Geophysics* **2020,** *58* (4), e2019RG000678.

2.   Rohling, E. J.; Rohling, E. J.; Sluijs, A.; Dijkstra, H. A.; Köhler, P.; van de Wal, R. S. W.; von der Heydt, A. S.; Beerling, D. J.; Berger, A.; Bijl, P. K.; Crucifix, M.; DeConto, R.; Drijfhout, S. S.; Fedorov, A.; Foster, G. L.; Ganopolski, A.; Hansen, J.; Hönisch, B.; Hooghiemstra, H.; Huber, M.; Huybers, P.; Knutti, R.; Lea, D. W.; Lourens, L. J.; Lunt, D.; Masson-Delmotte, V.; Medina-Elizalde, M.; Otto-Bliesner, B.; Pagani, M.; Pälike, H.; Renssen, H.; Royer, D. L.; Siddall, M.; Valdes, P.; Zachos, J. C.; Zeebe, R. E.; Members, P. P., Making sense of palaeoclimate sensitivity. *Nature* **2012,** *491* (7426), 683-691.

3.   Song, C., Global challenges and strategies for control, conversion and utilization of CO2 for sustainable development involving energy, catalysis, adsorption and chemical processing. *Catalysis Today* **2006,** *115* (1), 2-32.

4.   White, J. L.; Baruch, M. F.; Pander, J. E.; Hu, Y.; Fortmeyer, I. C.; Park, J. E.; Zhang, T.; Liao, K.; Gu, J.; Yan, Y.; Shaw, T. W.; Abelev, E.; Bocarsly, A. B., Light-Driven Heterogeneous Reduction of Carbon Dioxide: Photocatalysts and Photoelectrodes. *Chemical Reviews* **2015,** *115* (23), 12888-12935.

5.   Cohen, K. Y.; Evans, R.; Dulovic, S.; Bocarsly, A. B., Using Light and Electrons to Bend Carbon Dioxide: Developing and Understanding Catalysts for CO_2 Conversion to Fuels and Feedstocks. *Accounts of Chemical Research* **2022,** *55* (7), 944-954.

6.   Elgrishi, N.; Chambers, M. B.; Wang, X.; Fontecave, M., Molecular polypyridine-based metal complexes as catalysts for the reduction of CO_2 *Chemical Society Reviews* **2017,** *46* (3), 761-796.

7.   Grice, K. A., Carbon dioxide reduction with homogenous early transition metal complexes: Opportunities and challenges for developing CO_2 catalysis. *Coordination Chemistry Reviews* **2017,** *336*, 78-95.

8.   Costentin, C.; Robert, M.; Savéant, J.-M.; Tatin, A., Efficient and selective molecular catalyst for the CO_2-to-CO electrochemical conversion in water. *Proceedings of the National Academy of Sciences* **2015,** *112* (22), 6882.

9.   Costentin, C.; Robert, M.; Savéant, J.-M., Catalysis of the electrochemical reduction of carbon dioxide. *Chemical Society Reviews* **2013,** *42* (6), 2423-2436.

10.   Stanbury, M.; Compain, J.-D.; Chardon-Noblat, S., Electro and photoreduction of CO_2 driven by manganese-carbonyl molecular catalysts. *Coordination Chemistry Reviews* **2018,** *361*, 120-137.

11.   Takeda, H.; Cometto, C.; Ishitani, O.; Robert, M., Electrons, Photons, Protons and Earth-Abundant Metal Complexes for Molecular Catalysis of CO_2 Reduction. *ACS Catalysis* **2017,** *7* (1), 70-88.

12.   Sinopoli, A.; La Porte, N. T.; Martinez, J. F.; Wasielewski, M. R.; Sohail, M., Manganese carbonyl complexes for CO_2 reduction. *Coordination Chemistry Reviews* **2018,** *365*, 60-74.

13.   Hernández, S.; Amin Farkhondehfal, M.; Sastre, F.; Makkee, M.; Saracco, G.; Russo, N., Syngas production from electrochemical reduction of CO_2: current status and prospective implementation. *Green Chemistry* **2017,** *19* (10), 2326-2346.

14.   Graves, C.; Ebbesen, S. D.; Mogensen, M.; Lackner, K. S., Sustainable hydrocarbon fuels by recycling CO_2 and H_2O with renewable or nuclear energy. *Renewable and Sustainable Energy Reviews* **2011,** *15* (1), 1-23.

15.   Hawecker, J.; Lehn, J.-M.; Ziessel, R., Efficient photochemical reduction of CO_2 to CO by visible light irradiation of systems containing Re(bipy)(CO)$_3$X or Ru(bipy)$_3{}^{2+}$–Co^{2+} combinations as homogeneous catalysts. *J. Chem. Soc., Chem. Commun.* **1983,** (9), 536-538.

16.   Clark, M. L.; Cheung, P. L.; Lessio, M.; Carter, E. A.; Kubiak, C. P., Kinetic and Mechanistic Effects of Bipyridine (bpy) Substituent, Labile Ligand, and Brønsted Acid on Electrocatalytic CO_2 Reduction by Re(bpy) Complexes. *ACS Catalysis* **2018,** *8* (3), 2021-2029.

17.   Smieja, J. M.; Kubiak, C. P., Re(bipy-tBu)(CO)3Cl−improved Catalytic Activity for Reduction of Carbon Dioxide: IR-Spectroelectrochemical and Mechanistic Studies. *Inorganic Chemistry* **2010,** *49* (20), 9283-9289.

18.   *CRC Handbook of Chemistry and Physics*. 92 ed.; CRC Press: Boca Raton, FL, 2011.

19.   Smieja, J. M.; Sampson, M. D.; Grice, K. A.; Benson, E. E.; Froehlich, J. D.; Kubiak, C. P., Manganese as a Substitute for Rhenium in CO_2 Reduction Catalysts: The Importance of Acids. *Inorganic Chemistry* **2013,** *52* (5), 2484-2491.

20.   Bourrez, M.; Molton, F.; Chardon-Noblat, S.; Deronzier, A., [Mn(bipyridyl)(CO)$_3$Br]: An Abundant Metal Carbonyl Complex as Efficient Electrocatalyst for CO_2 Reduction. *Angewandte Chemie International Edition* **2011,** *50* (42), 9903-9906.

21.   Grice, K. A.; Kubiak, C. P., Chapter Five - Recent Studies of Rhenium and Manganese Bipyridine Carbonyl Catalysts for the Electrochemical Reduction of CO_2. In *Advances in Inorganic Chemistry*, Aresta, M.; van Eldik, R., Eds. Academic Press: 2014; Vol. 66, pp 163-188.

22.   Tignor, S. E.; Kuo, H.-Y.; Lee, T. S.; Scholes, G. D.; Bocarsly, A. B., Manganese-Based Catalysts with Varying Ligand Substituents for the Electrochemical Reduction of CO_2 to CO. *Organometallics* **2019,** *38* (6), 1292-1299.

23.   Stor, G. J.; Morrison, S. L.; Stufkens, D. J.; Oskam, A., The Remarkable Photochemistry of fac-XMn(CO)3(.alpha.-diimine) (X =Halide): Formation of Mn2(CO)6(.alpha.-diimine)2 via the mer Isomer and Photocatalytic Substitution of X- in the Presence of PR3. *Organometallics* **1994,** *13* (7), 2641-2650.

24.   Bourrez, M.; Orio, M.; Molton, F.; Vezin, H.; Duboc, C.; Deronzier, A.; Chardon-Noblat, S., Pulsed-EPR Evidence of a Manganese(II) Hydroxycarbonyl Intermediate in the Electrocatalytic Reduction of Carbon Dioxide by a Manganese Bipyridyl Derivative. *Angewandte Chemie International Edition* **2014,** *53* (1), 240-243.

25.   Agarwal, J.; Shaw, T. W.; Stanton, C. J.; Majetich, G. F.; Bocarsly, A. B.; Schaefer, H. F., NHC-Containing Manganese(I) Electrocatalysts for the Two-Electron Reduction of CO_2 *Angewandte Chemie International Edition* **2014,** *53* (20), 5152-5155.

26.   Agarwal, J.; Shaw, T. W.; Schaefer, H. F., 3rd; Bocarsly, A. B., Design of a Catalytic Active Site for Electrochemical CO_2 Reduction with Mn(I)-Tricarbonyl Species. *Inorg Chem* **2015,** *54* (11), 5285-94.

27.   Stanton, C. J., III; Vandezande, J. E.; Majetich, G. F.; Schaefer, H. F., III; Agarwal, J., Mn-NHC Electrocatalysts: Increasing π Acidity Lowers the Reduction Potential and Increases the Turnover Frequency for CO_2 Reduction. *Inorganic Chemistry* **2016,** *55* (19), 9509-9512.

28.   Sampson, M. D.; Nguyen, A. D.; Grice, K. A.; Moore, C. E.; Rheingold, A. L.; Kubiak, C. P., Manganese Catalysts with Bulky Bipyridine Ligands for the Electrocatalytic Reduction of Carbon Dioxide: Eliminating Dimerization and Altering Catalysis. *Journal of the American Chemical Society* **2014,** *136* (14), 5460-5471.

29.   Sampson, M. D.; Kubiak, C. P., Manganese Electrocatalysts with Bulky Bipyridine Ligands: Utilizing Lewis Acids To Promote Carbon Dioxide Reduction at Low Overpotentials. *Journal of the American Chemical Society* **2016,** *138* (4), 1386-1393.

30.   Bhattacharya, M.; Sebghati, S.; VanderLinden, R. T.; Saouma, C. T., Toward Combined Carbon Capture and Recycling: Addition of an Amine Alters Product Selectivity from CO to Formic Acid in Manganese Catalyzed Reduction of CO_2. *Journal of the American Chemical Society* **2020,** *142* (41), 17589-17597.

31.   Franco, F.; Cometto, C.; Nencini, L.; Barolo, C.; Sordello, F.; Minero, C.; Fiedler, J.; Robert, M.; Gobetto, R.; Nervi, C., Local Proton Source in Electrocatalytic CO_2 Reduction with [Mn(bpy–R)(CO)$_3$Br] Complexes. *Chemistry – A European Journal* **2017,** *23* (20), 4782-4793.

32.   Takeda, H.; Koizumi, H.; Okamoto, K.; Ishitani, O., Photocatalytic CO_2 reduction using a Mn complex as a catalyst. *Chem. Commun.* **2014,** *50* (12), 1491-1493.

33.   Takeda, H.; Kamiyama, H.; Okamoto, K.; Irimajiri, M.; Mizutani, T.; Koike, K.; Sekine, A.; Ishitani, O., Highly Efficient and Robust Photocatalytic Systems for CO_2 Reduction Consisting of a Cu(I) Photosensitizer and Mn(I) Catalysts. *Journal of the American Chemical Society* **2018,** *140* (49), 17241-17254.

34.   Cheung, P. L.; Machan, C. W.; Malkhasian, A. Y. S.; Agarwal, J.; Kubiak, C. P., Photocatalytic Reduction of Carbon Dioxide to CO and HCO$_2$H Using fac-Mn(CN)(bpy)(CO)$_3$. *Inorganic Chemistry* **2016,** *55* (6), 3192-3198.

35.   Rohacova, J.; Ishitani, O., Rhenium(I) trinuclear rings as highly efficient redox photosensitizers for photocatalytic CO_2 reduction. *Chemical science* **2016,** *7* (11), 6728-6739.

36.   Cohen, K. Y.; Reinhold, A.; Evans, R.; Lee, T. S.; Kuo, H.-Y.; Nedd, D. G.; Scholes, G. D.; Bocarsly, A. B., Elucidating the mechanism of photochemical CO_2 reduction to CO using a cyanide-bridged di-manganese complex. *Dalton Transactions* **2022,** *51* (45), 17203-17215.

37.   Agarwal, J.; Stanton Iii, C. J.; Shaw, T. W.; Vandezande, J. E.; Majetich, G. F.; Bocarsly, A. B.; Schaefer Iii, H. F., Exploring the effect of axial ligand substitution (X = Br, NCS, CN) on the photodecomposition and electrochemical activity of [MnX(N–C)(CO)$_3$] complexes. *Dalton Transactions* **2015,** *44* (5), 2122-2131.

38.   Kuo, H.-Y.; S. Lee, T.; T. Chu, A.; E. Tignor, S.; D. Scholes, G.; B. Bocarsly, A., A cyanide-bridged di-manganese carbonyl complex that photochemically reduces CO_2 to CO. *Dalton Transactions* **2019,** *48* (4), 1226-1236.

39.   Kuo, H.-Y.; Tignor, S. E.; Lee, T. S.; Ni, D.; Park, J. E.; Scholes, G. D.; Bocarsly, A. B., Reduction-induced CO dissociation by a [Mn(bpy)(CO)$_4$][SbF$_6$] complex and its relevance in electrocatalytic CO_2 reduction. *Dalton Transactions* **2020,** *49* (3), 891-900.

40.   Ault, B. S.; Becker, T. M.; Li, G. Q.; Orchin, M., The infrared spectra and theoretical calculations of frequencies of fac-tricarbonyl octahedral complexes of manganese(I). *Spectrochimica Acta Part A: Molecular and Biomolecular Spectroscopy* **2004,** *60* (11), 2567-2572.

41.   Carriedo, G. A.; Carriedo, C.; Crespo, C.; Gómez, P., Synthesis of new neutral and cationic monocarbonyl complexes of manganese with bipyridine ligands. *Journal of Organometallic Chemistry* **1993,** *452* (1), 91-96.

42.   Machan, C. W.; Stanton, C. J.; Vandezande, J. E.; Majetich, G. F.; Schaefer, H. F.; Kubiak, C. P.; Agarwal, J., Electrocatalytic Reduction of Carbon Dioxide by Mn(CN)(2,2′-bipyridine)(CO)$_3$: CN Coordination Alters Mechanism. *Inorganic Chemistry* **2015,** *54* (17), 8849-8856.

43.   Yempally, V.; Moncho, S.; Hasanayn, F.; Fan, W. Y.; Brothers, E. N.; Bengali, A. A., Ancillary Ligand Effects upon the Photochemistry of Mn(bpy)(CO)$_3$X Complexes (X = Br$^-$, PhCC$^-$). *Inorganic Chemistry* **2017,** *56* (18), 11244-11253.

44.   Carriedo, G. A.; Crespo, M. C.; Riera, V.; Valin, M. L.; Moreiras, D.; Solans, X., Synthesis of Mono and Binuclear Carbonyl Complexes of Manganese with Cyanide or Thiocyanate Ligands. X-ray Crystal Structure of [{fac-Mn(CO)$_3$(phen)}$_2$(u-CN)]PF$_6$*.

45.   Kokkes, M. W.; De Lange, W. G.; Stufkens, D. J.; Oskam, A., Photochemistry of metal—metal bonded complexes: III. MLCT photolysis of (CO) 5MM′(CO)$_3$(α-diimine)(M, M′= Mn, Re) in 2-Me-THF and THF at 293 K; Evidence of photocatalytic formation of [(Mn (CO)$_3$(α-diimine)(P(n-Bu)$_3$)]$^+$[M (CO)$_5$]$^-$ upon photolysis in the presence of P(n-Bu)$_3$. *Journal of Organometallic Chemistry* **1985,** *294* (1), 59-73.

46.   Kokkes, M. W.; De Lange, W. G. J.; Stufkens, D. J.; Oskam, A., Photochemistry of metal—metal bonded complexes: III. MLCT photolysis of (CO)$_5$MM′(CO)$_3$(α-diimine) (M, M′ = Mn, Re) in 2-Me-THF and THF at 293 K; Evidence of photocatalytic formation of [(Mn(CO)$_3$(α-diimine)(P(n-Bu)$_3$)]+ [M(CO)$_5$] - upon photolysis in the presence of P(n-Bu)$_3$. *Journal of Organometallic Chemistry* **1985,** *294* (1), 59-73.

47.   Hartl, F.; Rossenaar, B. D.; Stor, G. J.; Stufkens, D. J., Role of an electron-transfer chain reaction in the unusual photochemical formation of five-coordinated anions [Mn(CO)$_3$(α-diimine)]$^-$ from fac-[Mn (X)(CO) $_3$(α-diimine)](X= halide) at low temperatures. *Recueil des Travaux Chimiques des Pays‑Bas* **1995,** *114* (11-12), 565-570.

48.   Reddy, K. S.; Yonetani, T.; Tsuneshige, A.; Chance, B.; Kushkuley, B.; Stavrov, S. S.; Vanderkooi, J. M., Infrared Spectroscopy of the Cyanide Complex of Iron(II) Myoglobin and Comparison with Complexes of Microperoxidase and Hemoglobin. *Biochemistry* **1996,** *35* (17), 5562-5570.

49.   Kosanovich, A. J.; Shih, W.-C.; Ozerov, O. V., Synthesis and characterization of unsaturated Manganese(I) and Rhenium(I) dicarbonyl complexes supported by an anionic PNP pincer. *Journal of Organometallic Chemistry* **2019,** *897*, 1-6.

50.   McKinnon, M.; Ngo, K. T.; Sobottka, S.; Sarkar, B.; Ertem, M. Z.; Grills, D. C.; Rochford, J., Synergistic Metal–Ligand Redox Cooperativity for Electrocatalytic CO_2 Reduction Promoted by a Ligand-Based Redox Couple in Mn and Re Tricarbonyl Complexes. *Organometallics* **2019,** *38* (6), 1317-1329.

51.   Scottwell, S. Ø.; Elliott, A. B. S.; Shaffer, K. J.; Nafady, A.; McAdam, C. J.; Gordon, K. C.; Crowley, J. D., Chemically and electrochemically induced expansion and contraction of a ferrocene rotor. *Chemical Communications* **2015,** *51* (38), 8161-8164.

52.   Frisch, M.; Trucks, G.; Schlegel, H.; Scuseria, G.; Robb, M.; Cheeseman, J.; Scalmani, G.; Barone, V.; Petersson, G.; Nakatsuji, H., Gaussian 16. Gaussian, Inc. Wallingford, CT: 2016.

53.   Zhao, Y.; Truhlar, D. G., The M06 suite of density functionals for main group thermochemistry, thermochemical kinetics, noncovalent interactions, excited states, and transition elements: two new functionals and systematic testing of four M06-class functionals and 12 other functionals. *Theoretical chemistry accounts* **2008,** *120* (1), 215-241.

54.   Calvinho, K. U. D.; Laursen, A. B.; Yap, K. M. K.; Goetjen, T. A.; Hwang, S.; Murali, N.; Mejia-Sosa, B.; Lubarski, A.; Teeluck, K. M.; Hall, E. S.; Garfunkel, E.; Greenblatt, M.; Dismukes, G. C., Selective CO_2 reduction to C3 and C4 oxyhydrocarbons on nickel phosphides at overpotentials as low as 10 mV. *Energy & Environmental Science* **2018,** *11* (9), 2550-2559.

55.   Jr., T. H. D., Gaussian Basis Functions for Use in Molecular Calculations. I. Contraction of (9s5p) Atomic Basis Sets for the First-Row Atoms. *The Journal of Chemical Physics* **1970,** *53* (7), 2823-2833.

56.   Slater, J. C.; Phillips, J. C., Quantum Theory of Molecules and Solids Vol. 4: The Self-Consistent Field for Molecules and Solids. *Physics Today* **1974,** *27* (12), 49-50.